Received: September 8, 2022. Revised: December 4, 2022.

INASS

International Journal of
Intelligent Engineering & Systems

http://www.inass.org/

Automatic Atrial Fibrillation Detection Using Modified Moth Flame Optimization Algorithm

Sreenivasulu Ummadisetty[1]* **Madhavi Tatineni[2]**

[1]*Department of Electrical, Electronics and Communication Engineering, GITAM School of Technology, Vishakapatnam, Andhra Pradesh, India*
[2]*Department of Electrical, Electronics and Communication Engineering, GITAM School of Technology, Hyderabad, India*
* Corresponding author's Email: summadis@gitam.edu

Abstract: The absence of P waves through electrocardiogram (ECG) tracing causes atrial fibrillation (AF) affecting around 1% of the global population. In recent years, wearable and portable devices have made mobile healthcare much closer to reality. The main purpose of this article is to develop an automatic AF detection system based on short single lead ECG signals. Also, AF is one kind of arrhythmia that change the rhythms in the heart and have the potential to alter the characteristics of morphology in ECG tracings. For feature extraction, heart rate variability (HRV) and frequency analysis are adopted. The novel contribution of this work is to deploy a modified Moth Flame Optimization algorithm for detecting AF in a short ECG recording. The obtained results were validated with the available public data set comprised of short ECG recordings by genetic algorithm and modified moth flame optimisation algorithm. For N versus A classification, accuracy varies from 94.2% to 97% under noise levels ranging from 0 to 30 dB. For N versus A versus O, maximum accuracy of 84.3% is obtained. The obtained experimental results suggest that HRV is efficient and robust for AF detection for relatively short ECG recording.

Keywords: Atrial fibrillation, ECG, Modified moth flame optimisation, Genetic algorithm.

1. Introduction

Atrial fibrillation (AF) disorder affects more than 5% of people aged over 65 in the world. AF is more in men compared to women. This AF is one kind of arrhythmia that might lead to heart stroke and even heart failure. Therefore, AF can be controlled and managed only with a timely diagnosis. The ion channel functions of cardiomyocytes (Remodelling) are adopted as a pathological condition for the patient's atrium after persistent AF. Experienced cardiologists in the clinical practice inspect manual tracing of ECG. The disadvantage of manual tracing of ECG is time consumption. Holter monitors acquire a long-term recording of ECG; that is very hard to locate the abnormal episodes by cardiologists. To overcome this problem, the development is needed for a robust as well as efficient decision-making system for automatic detection of atrial fibrillation (ADAF) required. Almost all decision support systems use inputs as ECG signals. These input signals were translated into useful features using an algorithm, and one final result is outputted for clinicians. Sahoo et al. [1] reviewed non-episodic ECG using different features of data analytics. In work [2], a new ECG monitoring system is developed with the use of portable self-designed low cost arduino sensor device. *Ferri, et al* [3] developed a new method for dry electrodes on textiles. The monitoring of health has actively included wearable technology. They make it possible to continuously monitor health indicators, creating countless opportunities. The development of algorithms for disease prediction, prevention, and intervention can benefit from wearable technology. *Li, et al* [4] utilized a flexible electro-optic polymer modulator for improving an ECG signal acquisition. *Yao, et al* [5] deployed an

effective coating strategy based electron conjunction for enhancing the stability and conductance. *Chen, et al* [6] implemented a Feed Forward Neural Network (FFNN) mechanism for developing an automated atrial fibrillation detection system. Here, the wavelet transform and sliding window based filtering techniques are applied for preprocessing the input ECG signals, which helps to reduce the level of noise. *Yildirim, et al* [7] developed a new deep learning approach for accurately detecting the cardiac arrhythmia from the ECG signals. In paper [8], a new classification approach, named as, Asymmetric Domain Adaptation Neural Network (ADANN) has been developed to improve the performance of AF detection system. Here, a Denoising Auto-Encoder (DAE) mechanism is utilized to resolve the data shift problem. *Jiang, et al* [9] used a multi-scale feature fusion model for detecting an AF from the ECG signals. *Marshili, et al* [10] formulated an optimized framework for the detection of AF from ECG signals. The contribution of this paper was to obtain an increased detection accuracy, reduced memory usage and time consumption. *Zhang, et al* [11] introduced a spatial temporal attention based convolutional recurrent neural network mechanism for detecting multiclass arrhythmia from the given ECG signals. In paper [12], a standard Artificial Neural Network (ANN) mechanism is employed to identify an AF with the help of portable devices. *Ganapathy, et al* [13] developed an automated AF detection system using ECG signals, where the dynamic symbolic assignment is also proposed to properly differentiate the normal rhythm from the AF. Since quick intervention in the effective detection of AF might prevent serious effects brought on by a development of the condition, machine learning has greatly contributed to the development of real-time monitoring of AF. The automatic classification of AF has progressed significantly due to technological innovations and artificial intelligence technology. The feature extraction and classification are the two components of the conventional ECG classification system. In the existing works, various optimization and classification methodologies are employed for developing an automated ECG signal processing system. Traditional models have several significant problems due to advances in artificial intelligence. Prior to combining machine learning algorithms for classification, conventional algorithms should first design feature extraction techniques to extract valuable information. Information loss may occur as a result of this process. The classification results could appear to have greater faults when the extracted features can't accurately reflect the data. Furthermore, it heavily depends on ample prior expert knowledge and adequate medical diagnostics processing abilities. On this premise, developing a good optimization [14-18] and classification technique is also essential, yet getting the best outcomes is challenging.

Numerous studies have demonstrated that adding optimization techniques [19-22] and machine learning features to the classifier would enhance system performance and produce more accurate classification results. Although the aforementioned research can successfully resolve the classification issue for AF, we can see that different neural networks can successfully extract complicated nonlinear characteristics from the original data without the need for human involvement. However, it is still challenging to learn the reasoning process behind the ECG signal features with the high accuracy needed for monitoring. Based on the survey, the following problems faced by the existing works are studied, which includes high misprediction, zero-frequency problem, overlapping, does not suitable for large datasets, and higher training time. Therefore the proposed work motivates to develop a novel optimization and classification models for an automated AF detection. The major research objectives of this paper are as follows:

- To attain an improved classification accuracy, the different types of signal features such as HRV based features, and spectral features are extracted.
- To optimally choose the most relevant parameters from the list of available features, an enhanced moth flame optimization algorithm is developed.
- To accurately identify and predict the AF from the given ECG signals based on its optimal features, the Support Vector Machine (SVM) classification algorithm is developed.
- To validate and test the performance of the proposed system, an extensive simulation and comparative analyses are carried out in this paper.

The original contribution of this proposed work is to develop a highly efficient and competent methodology for detecting AF from the given ECG signals. In this framework, the HRV based feature extraction methodology has been utilized to analyze the dynamic characteristics of the heart activities. Since, the HRV model is highly robust in nature, which also helps to obtain an increased detection accuracy and confidence. Moreover, the moth flame

optimization mechanism is used to optimally select the features from the set of available features, which increases the training rate and reduces the false prediction rate of classification. Then, an enhanced SVM model is applied to accurately detect the AF by training the optimized set of features. When compared to the other existing AF detection methodologies, the proposed AAFD has the major benefits of high detection accuracy, optimized performance, reduced complexity, increased training speed, and minimized time consumption.

2. Materials and methods

This research work aims to develop an efficient and robust AAFD method of data processing that is gathered from either wearable or portable devices under high noise environments. The data collected from those devices are generally vulnerable. It can have anticipated that the recording signals are available in smaller slices rather than a clean section of long signal. Furthermore, portable devices cannot attach to the patients and will not work similarly to the wearable fashion. The recording length usually depends on the patient's behaviour; therefore, it is unmanageable to process data for the developers. The morphological characteristics such as PR/ST intervals and QRS complex length are physiologically sound and clinically relevant but these features were not preferred as they were not suitable for the above-mentioned scenarios. R peak in ECG signal is usually the dominant fiducial point as it is the most unaffected feature compared with all other features. If there is no identification of R peaks in any segment of ECG, then it is difficult for the characteristics waves or other fiducial points to provide useful information. R peak can be detected with high accuracy and confidence for both low and moderate noise levels. Therefore, we considered HRV based features for dynamic characteristics of heart activities due to their robustness under noisy scenarios. The overall framework of the proposed method is depicted in Fig. 1.

2.1 Data description

The required data for this work is taken from the publicly available dataset which is released in 2017 by Computing in Cardiology Challenge (CinC). It consists of short ECG recordings (total number of 8528 recordings) of lengths ranging from 9 seconds to more than 1 minute that is measured with a single lead. Clinical cardiologists label these recordings as normal rhythm (N), atrial fibrillation (AF), other arrhythmias (O) and noisy (~). Table 1 and figure 2 show the dataset distribution and sample recordings. The classified dataset recording contains about 60% as normal rhythm, 9% as episodes of AF, and 28% as arrhythmias other than atrial fibrillation. The rest of the 3% data has been identified as being too noisy.

2.2 Feature extraction

2.2.1. HRV based features

The first step used for the detection of R peak is

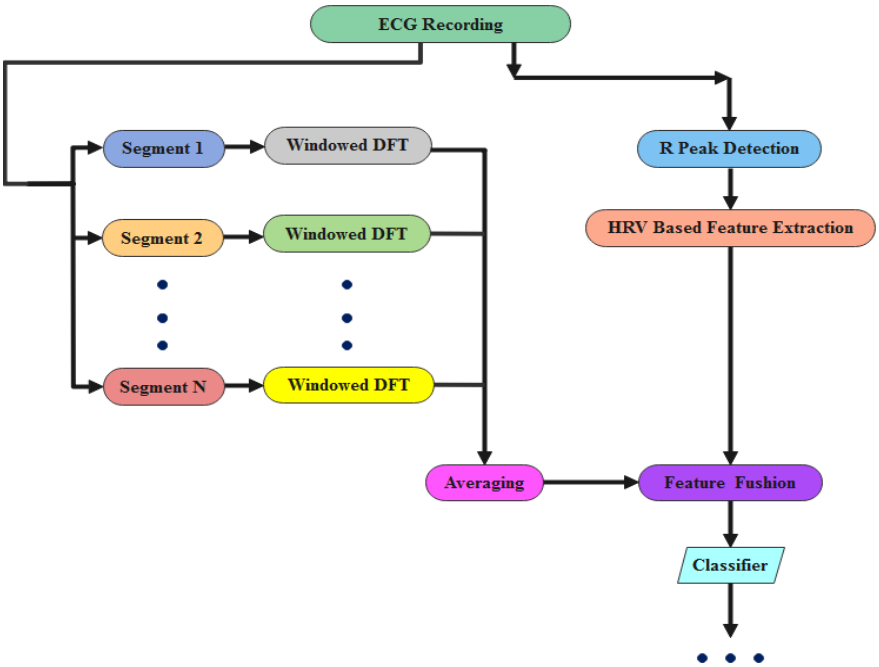

Figure. 1 The proposed method overall framework

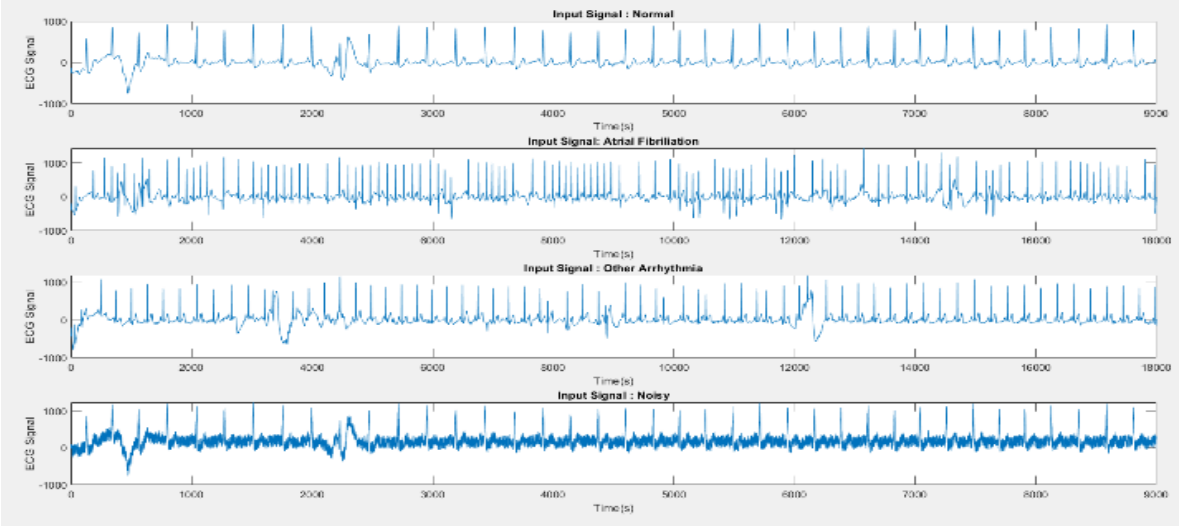

Figure. 2 Sample recordings for all four classes

Table 1. Dataset distribution of the sample recordings

Type	# Recordings	% portion
Normal Rhythm (N)	5076	59.52%
Atrial Fibrillation (AF)	758	8.89%
Other Arrhythmias (O)	2415	28.32%
Noisy (~)	279	3.27%
Total	**8528**	**100%**

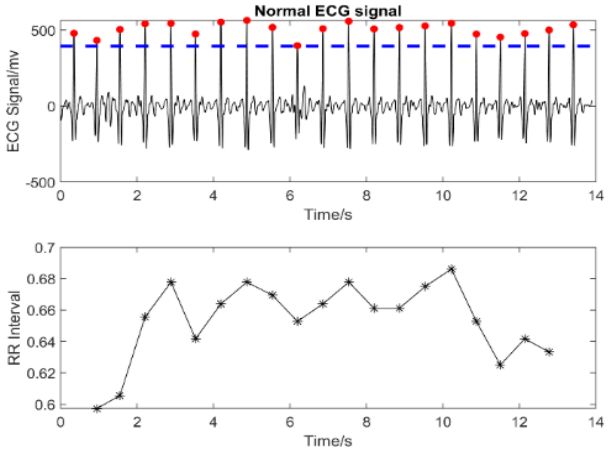

Figure. 3 HRV from ECG: (a) original signal (Top) (b) Inter pulse intervals as an unevenly spaced signal (Bottom)

to extract HRV based features. The average HR (beats/min) is calculated as $HR = 60 \times \frac{N.f}{L}$. Where N is the number of R peaks, f is the sampling signal frequency in Hz, and L is the length of the recording. N number of R peaks having N-1 intervals and the sequence of RRI is in order: $RRI = [RR_1, RR_2, \ldots . RR_{N-1}]$. Heart rate variability (HRV) is the variation in heart rate from beat-to-beat or the R–R interval duration, becoming a popular clinical and investigational tool. The frequency-domain in HRV relates to the energy distribution and autonomous nervous system (ANS) activities. The power spectrum density (PSD) of HRV contains a power-law relationship that can be obtained by plotting the logarithm of PSD against the logarithm of the frequency. This PSD interprets sympathetic-vagal balance. Fig. 3 despites the original ECG signal and RRI sequence as a function of time.

The normalised energy distribution for any given signal s(t) on the time axis as $\left(\int_{-\infty}^{\infty}|s(t)|^2 dt = 1\right)$, we have:

$$\left(\int_R t^2|s(t)|^2 dt\right).\left(\int_R f^2|\hat{s}(f)|^2 df\right) \leq \frac{1}{16\pi^2} \quad (1)$$

Where $\hat{s}(f)$ is the *Fourier transform* of s(t). The signals obtained from RRI sequences are compactable in the time domain, but the energy concentration signal is much poor in the corresponding frequency domain.

For the above-mentioned reasons, the estimation of the RRI sequences with high energy concentrations is used, and the direct power spectrum density is waived in this research work. The advantage of these Poincare plots is characterising the detailed dynamic information conceded. The first-order difference of RRI is denoted as dRR where $dRR_i = RR_{i+1} - RR_i$. For the Hankel matrix (A) defined as $[a_1, a_2, a_3, \ldots\ldots, a_n]$, is:

$$H = \begin{bmatrix} a_1 & a_2 & a_3 & \ldots & a_n \\ a_2 & a_3 & a_4 & \ldots & a_1 \\ . & . & . & . & . \\ . & . & . & . & . \\ . & . & . & . & . \\ a_{n-1} & a_n & a_1 & \ldots & a_{n-2} \\ a_n & a_1 & a_2 & \ldots & a_{n-1} \end{bmatrix} \quad (2)$$

The speciality of the Hankel matrix is each ascending skew-diagonal from left to right is a constant called *Hermitian symmetry*. Further, this matrix is diagonalised by a *unitary* matrix U:

$$H = U * DU \tag{3}$$

The diagonal matrix D consists of all the eigenvalues of H that are arranged along its diagonal line and * denotes the conjugate transpose. It was observed that the spectral radius of square matrix H is also central symmetry and the largest absolute value of its eigenvectors constituting U bases in the *Fourier* domain. Therefore, all the eigenvalues are arranged in ascending order. The matrix U is a permutation matrix which is a binary square matrix that consists of one entry of 1 exactly in each row and each column and elsewhere 0s. The rows and columns present in U and U* were permuted correspondingly. The feature map is symmetrical, and the structural irregularities are characterised. The matrix U contains a non-zero entry in the i_{th} column is denoted as I_i, $i \in 1, 2, \ldots\ldots, \frac{n}{2}$; the Hankel distance (HankDist) is defined as

$$\boldsymbol{HankDist} = \frac{4}{n^2}\sum_{i=1}^{\left[\frac{n}{2}\right]}|I_i - i| \tag{4}$$

The feature maps that contain non-zero entries are purely sinusoidal sequences that lie along the diagonal and anti-diagonal lines. The obtained matrix series of such Hankdist will be zero. For irregularly scattered feature maps, the HankDist is large. The HankDist is computed for both RRI and dRR. The standard descriptors [5] in the Poincare plot that contains SD_1, SD_2 and $SD_{ratio} = SD_1/SD_2$ are linear descriptor of the RRI sequence. For RRI consecutive pairs like (RR_1, RR_2), are plotted against RR_i. The data points from the normal RRI in the constructed Poincare plot lie along the straight-line y = x, and these data points are used to form an ellipse. The long axis (SD_1) of the ellipse replicates the long-term dispersion. In contrast, the short axis (SD_2) replicates the short-term distribution of the fluctuation of RRI, so also the dynamics of heart activity. To extract SD_1 and SD_2 the data points are rotated 45° in the clockwise direction. Denote $(x, y)^T = (RR_i, RR_{i+1})^T$ where i = 1, 2, ….., N-1 then:

$$\begin{bmatrix} x' \\ y' \end{bmatrix} = \begin{bmatrix} cos\frac{\pi}{4} & sin\frac{\pi}{4} \\ -sin\frac{\pi}{4} & cos\frac{\pi}{4} \end{bmatrix} \cdot \begin{bmatrix} x \\ y \end{bmatrix} \tag{5}$$

The new data points were donated with $(x', y')^T$ whereas the variance along x' axes is computed as SD_1, and $SD_2^2 = 2.Var(RR) - SD_1^2$. The Poincare plot is discovered as a nonlinear analysis tool, but the descriptors (SD_1, SD_2) are a linear combination of the basic statistics of the original RRI sequence. The second-order statistics are applied to the original RRI series to determine not being nonlinear. However, the above descriptors were invariant, implying the limited ability to reflect the order structure in RRI. The area occupied by 3 consecutive RRI pairs is used for the calculation of 'generation' (after possible delay-embedding). The area occupied by ((RR_i, RR_{i+1}) → (RR_{i+1}, RR_{i+2}) → (RR_{i+2}; RR_{i+3})) is denoted with A(i), we have:

$$A(i) = \begin{vmatrix} RR_i & RR_{i+1} & 1 \\ RR_{i+1} & RR_{i+2} & 1 \\ RR_{i+2} & RR_{i+2} & 1 \end{vmatrix} \tag{6}$$

And CCM is the normalised area that is occupied:

$$CCM = \frac{1}{K\pi SD_1.SD_2}.\sum_{i=1}^{K} A(i) \tag{7}$$

Apart from RRI, the power spectrum distribution (PSD) characteristics with frequency interpretation of components are expectable [5]. But this PSD from the difference of RRI sequences (δRR) shows that it failed to provide significant variation w.r.t white noise. But it is observed that δRR is capable to distinguish AF from normal rhythm.

2.2.2. Spectral feature

One main disadvantage of HRV based features is that they only contain information on heart activities in the sketch. ECG contains detailed morphology. It is vulnerable to noise; therefore, it is better not to characterise the characteristic waves (CW) in the time domain, but the frequency domain has a relatively stable structure. The estimation of Welch PSD is simply a minor modification to the periodogram method. The estimation of reduced variance is obtained in Welch PSD compared to the periodogram method with the expense of lowering frequency resolution. Assume one uniform ECG sample signal of total length N. This signal is divided into M segments equally with each length L with or without overlapping. The overlapping is denoted with D; we have:

$$L + (M-1)(L-D) = N \tag{8}$$

A windowed discrete fourier transform (DFT) is calculated for each segment $X_k(i)$, where i = 0, 1, ….., L-1, is as follows:

$$\hat{P}_k(n) = \frac{1}{L}\sum_{i=0}^{L-1} X_k(i)W(i)e^{-2\Pi ji\frac{n}{L}}, \quad k = 1,2,\dots,M \tag{9}$$

Where W(i) denotes the window function that aims to reduce the frequency leakage. Finally, the spectral estimation is scaled into $\left[\frac{-1}{2},\frac{1}{2}\right]$ which is the normalised average of all the M periodograms above:

$$\hat{p}\left(\frac{n}{L}\right) = \frac{1}{M}\sum_{k=1}^{M}\frac{|L.\hat{P}_k(n)|^2}{W_0}, n = 1,2,\dots,\frac{L}{2} \tag{10}$$

here W_0 is the energy of the window function:

$$W_0 = \sum_{i=0}^{L-1}|W(i)|^2 \tag{11}$$

The frequency resolution is thus reduced from $\frac{N}{2}$ to $\frac{L}{2}$. However, the estimation's variance is reduced by a factor of up to M. The order of magnitude of N in our case is about 10^3 – 10^4. If M's order of magnitude is about 10^1, considering the sampling frequency is 300 Hz (so the power spectrum will be distributed in 0-150 Hz), we still have a resolution level of about 1 frequency point/Hz.

2.2.3. Selection of features

This work uses maximum-relevance-min-redundancy (MRMR) which is based on mutual information. As the name indicates, this model can maximise relevance while minimising the redundancies between the features and the targets (labels). The mutual information is used to estimate the relevance and redundancy. The set of all the original features and the set of the selected features are denoted with Ω and S respectively. The feature selection is used to discover the optimal subset S of cardinality m which is:

$$Objective\ Function = \underset{S\subseteq\Omega}{arg\,max}\, I(S_m,t) \tag{12}$$

Where t as the targets (labels), I (. , .) as the mutual information estimation and |.| as the cardinality operator. A straightforward selection procedure that uses an exhaustive search is considered an impractical choice to find out combinatorial subset S. Also, the mutual information is difficult to estimate for the high dimensional variable.

2.2.3.1. Feature selection with modified moth flame optimisation algorithm

To avoid local optimisation and find the global update, the moth flame optimisation algorithm is further modified with a levy flight mechanism. Now, this algorithm expands the search scope, and hence this algorithm is named as modified moth flame optimisation algorithm. The improved formula is:

$$S(M_i, F_j) = D_i.e^{bt}.\cos(2\pi t) + L(d).F_j \tag{13}$$

Where M_i and F_j are i^{th} moth and j^{th} flame respectively. D_i is the distance between the i^{th} moth and j^{th} flame. The current iteration number is denoted with t. The spiral flight of the moth updates its position with the addition of the levy flight mechanism, which expands the search range and prevents the moth from falling into local optimisation. The levy flight formula is as follows.

$$Levy(x) = 0.01\frac{r_1\delta}{|r_2|^{\frac{1}{\varphi}}} \tag{14}$$

Where r_1 and r_2 are the random numbers between [0,1], φ is a constant 1.5, and the δ formula is as follows:

$$\delta = \left(\frac{\tau(1+\varphi)\sin\left(\frac{\pi\varphi}{2}\right)}{\tau\left(\frac{1+\varphi}{2}\right)\varphi 2^{\left(\frac{\varphi-1}{2}\right)}}\right)^{\frac{1}{\varphi}} \tag{15}$$

The modified moth flame optimisation algorithm is as follows:

Algorithm 1: Modified moth flame optimisation code

1: Initialisation of the Moths
2: For I =1: N
3: For j = 1:D then
4: $MO_{i,j}$ = random position between given bounds;
5: end
6: O = Fitness value
7: end
8: C = 1
9: While $MO_i = |FO_j - MO_i| * e^{bt}\cos(2\pi t) + FO_j$
10: If $C\_iter \le T\_iter$
11: MO_i = Fitness value (MO_i)
12: Elseif $C\_iter == 1$
13: FO = Quick Sort (MO)
14: O_{FO}= Quick Sort (O_{MO})
15: Else
16: FO = Quick Sort (MO_C , MO_{Citer})

17: O_{FO} = Quick Sort($MO_{Citeer-1}$, MO_{Citer})
18: End
19: Update b and t
20: $MO_i = |FO_j - MO_i| * e^{bt} \cos(2\pi t) + FO_j$
21: Update the number of flames
22: $N = ceil\left(N - C_{iter} * \frac{N-1}{T_{iter}}\right)$
23: $C_{iter} = C_{iter} + 1$
24: End
25: Exit

2.2.4. Feature optimisation

In this instigation, the fitness function used must satisfy the simultaneous maximisation of relevance (R_V) and minimisation of redundancy (R_D). Therefore, the fitness function (F) was directly proportional to R_V and inversely proportional to R_D.

$$\Rightarrow F \propto R_V \quad and \quad F \propto \frac{1}{R_D}$$
$$F = \underset{S\subseteq\Omega,|S|=m}{arg\,max}(R_V - R_D) \quad or \quad \frac{R_V}{R_D} \tag{16}$$

Relevance R_V and redundancy R_D are defined as follows:

$$R_V = \frac{1}{|S|} \sum_{i\epsilon S} I(i,t) \tag{17}$$

$$R_D = \frac{1}{|S|^2} \sum_{i,j\epsilon S} I(i,j) \tag{18}$$

2.2.5. Additional noise resistance test

The data set contains 279 recordings under noisy class readings, around 3.27%, which is a relatively smaller proportion that can be easily excluded. The robustness of this model against noise is investigated by introducing the different intensities added artificially. Fig. 5 shows the original sample recording and noise corrupted versions. The signal to noise ratio (SNR) for the existing original noise recordings does not have a reliable estimation, so original signals are taken as clean signals. Then we use all the energy from the original recordings to compute P_s, and white noise of power P_n is added. The SNR is:

$$SNR = 10.log\frac{P_s}{P_n} dB \tag{19}$$

And the whole framework depicted in Fig. 1 will be performed under each noise level.

The obtained feature values corresponding to all the noise levels were trained. Genetic algorithm (GA) and modified moth flame optimisation algorithm (MMFOA) are used as classifiers. The test data set is separately not available publicly.

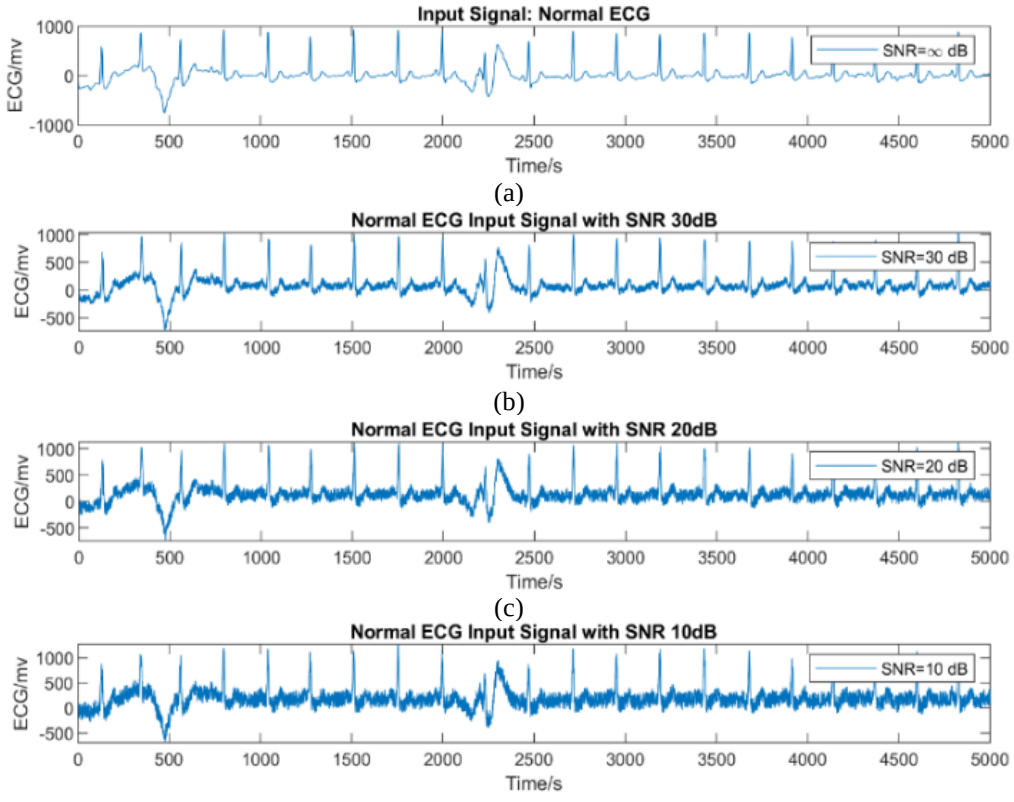

Figure. 5 NOISE TEST (a) SNR = ∞ dB (original signal), (b) SNR = 30 dB, (c) SNR = 20 dB, and (d) SNR = 10 dB

Therefore, the performance of classifiers was tested using k-fold cross-validation (k = 10). Then 30% of data of each subset (N, A, O) are reserved. Only 70% of data was involved in training and validation. The performances on the remaining 30% of data are reported to demonstrate the generalisation ability. All the computations are performed on Matlab2021a for 10 times, and averaged values are reported.

3. Results and discussions

3.1 Descriptive analysis

The pre-processing of each recording was carried out to obtain the feature vector. The power spectrum density and HRV based features were estimated from 0 Hz to 80 Hz. A 41-dimension feature vector was obtained after pre-processing. All the top-ranked features under noise levels are almost linear descriptors from the HRV analysis. At a high noise level (SNR = 10dB), the signals were disturbed, leading to slight variation in the different rankings. The performance metrics decrease as the noise level increases. The results obtained from the top 10 features were compared with all features.

The top 10 features selected by MMF-MRMR associated with each noise level are tabulated in Table 2. Under different noise levels, it is observed that the top-ranked features are linear and nonlinear descriptors based on HRV analysis. When SNR = 10 dB, the noise might disturb the RRI and lead to a different ranking. After selecting the top 10 features with a model-free feature selection scheme, the remaining low ranked features were eliminated. As the noise level increases, the performance metrics decrease slightly for almost all classification problems. The results obtained with the artificial test set were tabulated in table 4 for various noises, features and classification. For this analysis, the different types of existing techniques such as BT, SVM, and GA-MRMR are compared with the proposed model. These are all the standard meta-heuristics optimization based classification mechanisms used for detecting AF from the ECG signals. Moreover, these techniques have the major problems of increased over-fitting, training complexity, high time consumption, and slow convergence. Therefore, the proposed AAFD framework outperforms the other models with increased performance values. Also, these results were compared with different classifiers from the literature [23]. It is observed that, under all noise conditions, MMFOA is superior in terms of its performance and can be widely adopted for wearable devices.

Table 2. Top 10 features selected by MMF-MRMR

Rank	SNR=∞dB	SNR=30dB	SNR=20dB	SNR=10dB
1	AFE_V	AFE_V	AFE_V	RR_{mean}
2	CCM	SD_{ratio}	CCM	CCM
3	SD_{ratio}	CCM	SD_{ratio}	SD_{ratio}
4	RR_{mean}	RR_{mean}	$HANK_{RR}$	RR_{STD}
5	$PSD_{4.6-6.9}$	RR_{STD}	RR_{mean}	$PSD_{6.9-9.2}$
6	RR_{STD}	$HANK_{RR}$	$PSD_{6.9-9.2}$	$PSD_{2.3-4.6}$
7	$HANK_{RR}$	$PSD_{6.9-9.2}$	$PSD_{9.2-11.5}$	AFE_V
8	$PSD_{6.9-9.2}$	$PSD_{9.2-11.5}$	$PSD_{11.5-13.8}$	$PSD_{9.2-11.5}$
9	$PSD_{9.2-11.5}$	$PSD_{11.5-13.8}$	$PSD_{13.8-16.1}$	$PSD_{2.3-4.6}$
10	$PSD_{11.5-13.8}$	$PSD_{2.3-4.6}$	$PSD_{16.1-18.4}$	$PSD_{1.5-13.8}$

3.2 Descriptive analysis

Sensitivity, Specificity, and Accuracy are well-defined and reported for two-class classification problems. $Sen = \frac{TP}{TP+FN}$ (20)

$$Spec = \frac{TN}{TN+FP} \quad (21)$$

$$Acc = \frac{TP+TN}{TP+TN+FP+FN} \quad (22)$$

For two-class classification problems, the maximum accuracy is obtained for N/A recordings compared with both O/A and N/O recordings for the MMF-MRMR classifier. It is observed that the N/A recordings having the highest accuracies of 96.4% and 97% for GA-MRMR and MMF-MRMR respectively are obtained due to the sensitivity of nonlinear descriptors to arrhythmias. The results of this work are compared with BT and SVM [33] classifiers and found the accuracy of MMF-MRMR is more for all two-class classification problems than for the other three classifiers. The accuracies degrade with the increment in the SNR. For 10 dB SNR, the accuracy obtained is 95.3% using all features. For N/A top 10 features, the maximum and minimum accuracies are 96.7% and 94.5%, respectively. Also, it is observed that for O/A and N/O classification problems, the accuracy is dropped by about 5–9%. For the three-class classification problem, we defined the A as a positive class and N and O as negative classes and

counterparts of Sen and Spec are defined as the quotient of true positive/negative examples and all positive/negative examples and reported. For N/O/A, the highest accuracy of 84.3% is achieved with high specificities. The performance metrics of this class

Table 3. Comparison of classifier and classification performances on the test set under different configurations for different tasks

SNR	FEATURES	CLASSIFIER	N/A			O/A			N/O			N/O/A		
			Acc	Sen	Spec	Acc	Sen	Spec	Acc	Sen	Spec	Acc	Sen	Spec
∞dB	All	BT	96.6	83.2	98.6	89.0	69.3	95.3	84.7	68.1	92.5	81.8	64.6	98.1
		SVM	95.3	74.3	98.5	89.1	67.5	95.9	82.7	62.5	92.3	79.7	63.2	98.2
		GA-MRMR	96.4	79.7	99.1	92.0	75.3	98.1	85.2	68.3	94.9	82.8	71.6	99.3
		MMF-MRMR	97.0	82.0	99.3	92.8	77.0	98.7	86.5	70.4	95.4	84.3	73.4	99.4
	Top 10	BT	95.9	83.7	97.7	89.6	76.2	93.8	80.7	63.5	88.9	78.2	72.0	96.7
		SVM	96.2	82.6	98.2	89.7	74.6	94.4	80.3	61.6	89.2	78.2	73.0	97.3
		GA-MRMR	96.5	85.0	98.3	90.7	77.6	95.1	81.6	63.9	91.3	80.1	75.9	98.2
		MMF-MRMR	96.7	86.5	98.3	91.6	79.9	95.6	82.8	66.2	91.6	82.6	78.2	98.2
30dB	All	BT	96.6	83.2	98.6	89.3	70.5	95.3	84.7	68.3	92.5	82.0	69.3	97.9
		SVM	95.8	76.3	98.8	90.0	72.6	95.5	82.7	64.9	91.2	80.2	68.6	98.0
		GA-MRMR	96.4	78.4	99.1	91.4	72.1	97.8	85.0	67.4	94.3	82.5	68.4	98.8
		MMF-MRMR	96.9	81.3	99.3	92.2	73.0	98.4	86.1	69.1	95.1	84.4	72.1	99.0
	Top 10	BT	96.3	83.3	98.3	89.8	76.3	94.0	80.6	62.2	89.4	78.5	72.8	96.9
		SVM	96.4	83.6	98.3	89.6	75.0	94.2	80.0	59.7	89.7	78.0	73.5	97.2
		GA-MRMR	96.3	84.2	98.2	90.7	76.5	95.1	81.2	61.9	90.3	80.5	75.2	98.1
		MMF-MRMR	96.6	85.8	98.3	91.5	78.6	95.6	82.0	63.9	90.6	82.7	77.3	98.2
20dB	All	BT	96.3	82.2	98.4	89.7	70.4	95.9	83.8	66.3	92.2	81.1	66.0	98.1
		SVM	95.3	74.3	98.4	89.5	69.7	95.7	81.9	64.5	90.2	79.3	65.7	98.1
		GA-MRMR	96.2	76.4	98.9	91.3	70.5	97.4	84.2	65.4	93.3	82.7	68.2	98.7
		MMF-MRMR	96.4	77.4	99.2	91.9	72.4	97.8	85.1	67.1	94.1	84.3	69.7	99.0
	Top 10	BT	96.2	84.0	98.0	90.1	74.9	94.9	79.8	60.6	88.9	77.5	72.7	97.0
		SVM	95.9	82.4	97.9	88.6	72.5	93.6	78.7	58.9	88.1	76.4	71.0	96.9
		GA-MRMR	96.3	83.7	98.2	89.6	74.4	94.8	80.1	60.9	89.9	80.6	72.4	98.0
		MMF-MRMR	96.6	84.9	98.3	90.7	76.2	95.3	81.5	62.9	90.6	83.2	73.6	98.0

problem decrease slightly with the increase in the noise levels under all classifier configurations. The accuracy is comparable even after eliminating 80% of the low-ranked features and considering only the top 20% features. This validates our model-free feature selection based on mutual information. Considering only the top 10 features decreases the computational effect and inference time in ECG. Therefore, this algorithm can be anticipated for adoption in wearable devices.

4. Conclusion

This proposed work's novel contribution is the creation of a highly effective and qualified methodology for detecting AF from the provided ECG signals. The dynamic properties of the cardiac activity have been analysed in this framework using the HRV-based feature extraction methodology. The HRV model's high level of robustness contributes to improved detection confidence and accuracy. Additionally, the moth flame optimization process is utilised to choose the features from the collection of accessible features in the best way possible, which boosts training rates and lowers classification false prediction rates. Then, using the refined collection of characteristics, an improved SVM model is used to precisely detect the AF. The proposed AAFD algorithm detects AF even for short recordings of ECG. The long-term ECG recording for diagnosis is practically impossible as they experience various noises and artifacts. The validation of this algorithm is done on a publicly released dataset which comprises short ECG recordings from portable devices acquired under unstructured environments. This algorithm gives superior accuracy and specificity, making it compete with the prototype for preliminary screening. This research work is well-supported the effectiveness of the HRV based nonlinear features used for AF detection with short ECG recordings. Considering the existence of arrhythmias other than AF, cascading classification can be a direction of future work.

Conflicts of Interest

The authors declare that they have no conflict of interest.

Author Contributions

Methodology and software, SU; formal analysis and validation, MT; writing- original draft preparation, SU; Supervision, MT.

References

[1] S. K. Sahoo, W. Lu, S. D. Teddy, D. Kim, and M. Feng, “Detection of atrial fibrillation from non-episodic ECG data: a review of methods”, In: *Proc. of 2011 Annual International Conference of the IEEE Engineering in Medicine and Biology Society*, pp. 4992-4995, 2011.

[2] Y. Maithani, A. Singh, B. Mehta, and J. Singh, “PEDOT: PSS treated cotton-based textile dry electrode for ECG sensing”, *Materials Today: Proceedings*, 2022.

[3] J. Ferri, R. Llinares, I. Segarra, A. Cebriánv, E. G. Breijo, and J. Millet, “A new method for manufacturing dry electrodes on textiles. Validation for wearable ECG monitoring”, *Electrochemistry Communications*, Vol. 136, p. 107244, 2022.

[4] H. Li, Z. Lin, Y. Wang, Z. An, S. Zhang, Z. Zhang, “Demonstration of a flexible electro-optic polymer modulator with a low half-wave Voltage for ECG signals acquisition”, *Optics & Laser Technology*, Vol. 153, p. 108253, 2022.

[5] B. Yao, L. S. D. Vasconcelos, Q. Cui, A. Cardenas, Y. Yan, and Y. Du, “High-stability conducting polymer-based conformal electrodes for bio-/iono-electronics”, *Materials Today*, Vol. 53, pp. 84-97, 2022.

[6] Y. Chen, C. Zhang, C. Liu, Y. Wang, and X. Wan, “Atrial Fibrillation Detection Using a Feedforward Neural Network”, *Journal of Medical and Biological Engineering*, Vol. 42, pp. 63-73, 2022.

[7] Ö. Yıldırım, P. Pławiak, R. S. Tan, and U. R. Acharya, “Arrhythmia detection using deep conVolutional neural network with long duration ECG signals”, *Computers in Biology and Medicine*, Vol. 102, pp. 411-420, 2018.

[8] N. Ammour, “Atrial fibrillation detection with a domain adaptation neural network approach”, In: *Proc. of 2018 International Conference on Computational Science and Computational Intelligence (CSCI)*, pp. 738-743, 2018.

[9] F. Jiang, C. Hong, T. Cheng, H. Wang, B. Xu, and B. Zhang, “Attention-based multi-scale features fusion for unobtrusive atrial fibrillation detection using ballistocardiogram signal”, *BioMedical Engineering OnLine*, Vol. 20, pp. 1-21, 2021.

[10] I. A. Marsili, L. Biasiolli, M. Masè, A. Adami, A. O. Andrighetti, and F. Ravelli, “Implementation and validation of real-time algorithms for atrial fibrillation detection on a

wearable ECG device", *Computers in Biology and Medicine*, Vol. 116, p. 103540, 2020.

[11] J. Zhang, A. Liu, M. Gao, X. Chen, X. Zhang, and X. Chen, "ECG-based multi-class arrhythmia detection using spatio-temporal attention-based conVolutional recurrent neural network", *Artificial Intelligence in Medicine*, Vol. 106, p. 101856, 2020.

[12] D. Marinucci, A. Sbrollini, I. Marcantoni, M. Morettini, C. A. Swenne, and L. Burattini, "Artificial neural network for atrial fibrillation identification in portable devices", *Sensors*, Vol. 20, p. 3570, 2020.

[13] N. Ganapathy, D. Baumgärtel, and T. M. Deserno, "Automatic detection of atrial fibrillation in ECG using co-occurrence patterns of dynamic symbol assignment and machine learning", *Sensors*, Vol. 21, p. 3542, 2021.

[14] M. Dehghani, Z. Montazeri, A. Dehghani, R. A. R. Mendoza, H. Samet, and J. M. Guerrero, "MLO: Multi leader optimizer", *Int. J. Intell. Eng. Syst*, Vol. 13, pp. 364-373, 2020, doi: 10.22266/ijies2020.1231.32.

[15] F. A. Zeidabadi, M. Dehghani, and O. P. Malik, "TIMBO: Three influential members based optimizer", *International Journal of Intelligent Engineering and Systems*, Vol. 14, pp. 121-128, 2021, doi: 10.22266/ijies2021.1031.12.

[16] F. A. Zeidabadi, M. Dehghani, and O. P. Malik, "RSLBO: Random Selected Leader Based Optimizer", *International Journal of Intelligent Engineering and Systems*, Vol. 14, pp. 529-538, 2021, doi: 10.22266/ijies2021.1031.46.

[17] M. Sumanl, V. P. Sakthivel, and P. D. Sathya, "Squirrel search optimizer: nature inspired metaheuristic strategy for solving disparate economic dispatch problems", *International Journal of Intelligent Engineering and Systems*, Vol. 13, pp. 111-121, 2020, doi: 10.22266/ijies2020.1031.11.

[18] S. A. Doumari, H. Givi, M. Dehghani, and O. P. Malik, "Ring toss game-based optimization algorithm for solving various optimization problems", *International Journal of Intelligent Engineering and Systems*, Vol. 14, pp. 545-554, 2021, doi: 10.22266/ijies2021.0630.46.

[19] P. D. Kusuma and M. Kallista, "Stochastic Komodo Algorithm", *International Journal of Intelligence Engineering and Systems*, Vol. 15, pp. 156-166, 2022, doi: 10.22266/ijies2022.0831.15.

[20] P. D. Kusuma and A. Dinimaharawati, "Fixed Step Average and Subtraction Based Optimizer", *International Journal of Intelligent Engineering and Systems*, Vol. 15, 2022, doi: 10.22266/ijies2022.0831.31.

[21] F. A. Zeidabadi, S. A. Doumari, M. Dehghani, and O. P. Malik, "MLBO: Mixed Leader Based Optimizer for Solving Optimization Problems", *International Journal of Intelligent Engineering and Systems*, Vol. 14, pp. 472-479, 2021, doi: 10.22266/ijies2021.0831.41.

[22] F. A. Zeidabadi and M. Dehghani, "Poa: Puzzle optimization algorithm", *Int. J. Intell. Eng. Syst*, Vol. 15, pp. 273-281, 2022, doi: 10.22266/ijies2022.0228.25.

[23] Z. Mei, X. Gu, H. Chen, and W. Chen, "Automatic atrial fibrillation detection based on heart rate variability and spectral features", *IEEE Access*, Vol. 6, pp. 53566-53575, 2018.